Journal of Solid Mechanics Vol. 10, No. 2 (2018) pp. 285-299

# In-Plane and out of Plane Free Vibration of U-Shaped AFM Probes Based on the Nonlocal Elasticity

M. Ghadiri [1,*], S.A.H. Hosseini [2], M. Karami [1], M. Namvar [1]

[1]*Faculty of Engineering, Department of Mechanics, Imam Khomeini International University, Qazvin, Iran*
[2]*Department of Mechanics, Zanjan University, Zanjan, Iran*

Received 11 February 2018; accepted 3 April 2018

**ABSTRACT**

Atomic force microscope (AFM) has been developed at first for topography imaging; in addition, it is used for characterization of mechanical properties. Most researches have been primarily focused on rectangular single-beam probes to make vibration models simple. Recently, the U-shaped AFM probe is employed to determine sample elastic properties and has been developed to heat samples locally. In this study, a simplified analytical model of these U-shaped AFM is described and three beams have been used for modelling this probe. This model contains two beams are clamped at one end and connected with a perpendicular cross beam at the other end. The beams are supposed only in bending flexure and twisting, but their coupling allows a wide variety of possible dynamic behaviors. In the present research, the natural frequency and sensitivity of flexural and torsional vibration for AFM probes have been analyzed considering influence of scale effect. For this purpose, governing equations of dynamic behavior of U-shaped AFM probe are extracted based on Eringen's theory using Euler–Bernoulli beam theory and an analytical method is employed to solve these equations. The results in this paper have been extracted for different values of nonlocal parameters; it is shown that for a special case, there is a good agreement between reported results in available references and our results. The obtained results show that the frequencies of U-shaped AFM decrease with increasing the nonlocal parameter.



**Keywords:** U-shaped probe; AFM; Nonlocal elasticity theory; Euler–Bernoulli beam theory; Vibration analysis.

## 1 INTRODUCTION

MOST recently, many researchers have been interested increasingly in scanning and manipulating structures at nanometer scale. One of the strongly and useful tools in nano-scale technologies is atomic force microscopy (AFM), with applications from surface specifications in material science to the study of living biological systems. After Binnig et al. from IBM, which firstly presented the contact mode AFM in 1986, many AFM systems, have been presented [1-3]. Contact resonance in an atomic force microscope (AFM) has been used to quantify the elastic and viscoelastic properties for a variety of materials such as polymers, biological materials, ceramics, and metals with spatial resolution about tens of nanometers. In all these types of samples, a piezoelectric scanner scans a pointy probe at the end of a cantilever interacting locally with the sample. The dynamic AFM is utilized by moving the

*Corresponding author.
*E-mail address: ghadiri@eng.ikiu.ac.ir* (M.Ghadiri).

probe somewhat away from the sample surface and stumbling the probe at or near its topographical information of the natural resonance frequency of the sample and information on the tip–sample force action and reaction can be extracted by measuring the switch from its natural resonance frequency due to sample interactions [4-7]. It was shown that the flexural vibrations of micro cantilever probes were strongly influenced by the contact of the tip and the sample. This contact has been effectively "stiffened" the boundary condition for the beam and have increased the resonant frequencies. Measured shifts of the resonances were then modeled to determine the contact stiffness. In addition, the use of reference samples with known mechanical properties allowed these contact resonance AFM (CR-AFM);'approaches to produce more quantitative values within the limits of the beam vibration model (typically, an Euler-Bernoulli approach) and the tip-sample contact model [8-10]. Calculation of viscoelastic properties of polymers at the nano-scale was attracted attentions when a new type of AFM probe was developed in the late of 1990s. U-shaped AFM probes allow the probe tip to be heated locally such that the changes in the thermo-mechanical behavior of the sample can be modified or monitored. These probes have been used for specific applications such as storing thermo-mechanical data, growing carbon nanotubes by providing the required temperature and nano-scale manufacturing. Rabe et al. [11] studied the flexural vibration domain and the frequency of free and surface-coupled AFM cantilevers. Turner et al. [12] studied high-frequency answers of AFM cantilevers considering damping actions between the tip and the sample. Turner and Wiehn [13] centralized the sensitivity of vibration modes of AFM cantilevers to surface stiffness in both torsional and flexural vibrations. For simplicity, in all the above articles, it is supposed that the probe is equidistant to the sample surface, whilst in AFM joinery, a tilted cantilever is utilized which causes more complicated analysis. Chang[14] was successful in analysis of the sensitivity for the flexural vibration modes of the AFM cantilever. Considering the angle between the cantilever and the surface, inclusive of vertical and sidewise reaction forces, however, the tip–sample damping confined to the end of the beam has been ignored in his analysis. Damping in the tip-sample contact for the most elastic samples was not considerable and was usually ignored but this work found applications on multiple nano-scale materials similar to composite materials, glass [9, 15] dielectric materials, such as fluorosilicate glass (FSG)[16]ferroelectric ceramics[17-19] biological materials[18, 20] ferromagnetic materials, similar to yttrium iron garnet (YIG)[21]ultra-thin bort-like carbon coatings[22]and of course metals[23, 24]. Rabe et al. [8] have considered the damping effects using the elastic beam model, and comparing the results with solutions of the point-mass model. Besides the tip–sample damping, the damping of the probes is also very important. Two very different effects cause the damping of the cantilevers: system damping caused by internal casualties in the cantilever and by the surrounding air that affects all length elements of the beam in the same way. Mahdavi et al.[25] Have studied the high-frequency respond of AFM cantilevers using the elastic beam model and three different lumped models considering the damping of the cantilever. With lumped models, it is practical to model this inclusion tip–sample damping and derive the investigated solution, which is not simply practicable for the presented model. Barretta and Sciarra investigated Analogies between nonlocal and local Bernoulli–Euler Nano beams[26]. Romano et al. [27] showed that the nonlocal integral elastic law is equivalent to a problem composed of constitutive differential and boundary conditions. Also, Romano and Barretta[28] discussed the trueness of the proposed methodology for Eringen's nonlocal integral model for a bending Euler-Bernoulli and Timoshenko beams in details. Demir and Civalek studied on torsional and longitudinal frequency and wave response of microtubules based on the nonlocal continuum and nonlocal discrete models[29]. Gao introduced a new Timoshenko beam model incorporating microstructure and surface energy effects[30]. Civalek et al. studied Static analysis of single walled carbon nanotubes (SWCNT) based on Eringen's nonlocal elasticity theory[31]. Abbasi and Karami Mohammadi presented a new model for investigating the flexural vibration of an atomic force microscope cantilever[32]. In another investigations, Akgöz and Civalek studied on a new trigonometric beam model for buckling of strain gradient micro beams[33]. Also they investigated Vibration analysis of micro-scaled sector shaped graphene surrounded by an elastic matrix[34]. Lee and Chang presented Coupled lateral bending–torsional vibration sensitivity of atomic force microscope cantilever[35]. Muraoka[36] has proposed concentrated-mass cantilever to increase the sensitivity of the resonance frequency exceptionally for contacted with inflexible samples. He used a commercially available standard cantilever and a tungsten particle stickily attached to the free end. The cantilever boundary condition has been studied in many researches. Challamek et al. studied bending analysis of small scale bars based on some simplified nonlocal beam theory [37]. Moreover, Lim li et al. studied the nonlocal stress effect on a nano-cantilever considering axial torsion[38]. In addition, there have been studies based on clamp-free (cantilever) boundary conditions. Moreover, Narendar analyzed flatwise bending free vibration of a nanotube considering transverse shear deformation and rotating inertia on Eringen's nonlocal theory [39]. Recently, U-shaped AFM probes have been expanded to allow local heating of samples. The resonances of these probes are much more complex. Rezaei and Turner [40] studied a simplified analytical model of U-shaped probes.They used a three beam model analysis. Three-beam model analysis comprises two beams fixed at one end and attached with a vertical crossbeam at the other end. The beams are

supposed only to be bent in flexure and to be deformed, but their connection allows an extensive domain of doable dynamic conductance. Issues are expanded for ten primary modes and the mode shapes are shown to have made a difficult connection between the flexure and deform of the beams, especially for the higher modes. The results of the all resonant frequencies are in good agreement with finite element results for the three probe designs and two values of thickness examined [40].

In this article, the out-of-plane vibrations of a U-shaped atomic force microscope probe considering the effect of nonlocal are modeled analytically. The simplified approach assumes three beams that are allowed only to be bent in flexure and to twist no lateral motion is considered for simplicity. The model allows resonances and mode shapes to be determined with respect to geometry and material properties very efficiently so that the overall response can be more clearly understood. The results for this model, in terms of the resonant frequencies and mode shapes, are compared with results without considering the nonlocal effect. It is anticipated that this work will expand the capabilities of U-shaped atomic force microscope probes, so that, they can be used eventually for quantitative measurements of material properties using a contact resonance approach during heating.

## 2 THREE-BEAM MODEL (TBM)

The analytical model of a U-shaped probe is based on the Euler-Bernoulli beam theory. Parallel "legs" with the same length are assumed to be connected with a crossbeam. In this model, two legs are clamped at one end, and the cross beam is coupled to them at the opposite end. In reality, the U-shaped probes are fabricated from a single silicon wafer with uniform material properties such that the U-shaped probe is more like a plate. However, for the geometries typical for these probes, appropriate assumptions of the beams are satisfied [41].

## 3 NONLOCAL BEAM MOEL

Many researchers have focused on vibration analysis of the nanoscale structures using the nonlocal theory [42-51]. Nonlocal elasticity theory was firstly introduced by Eringen [52], and the stress field at a point $x$ in an elastic continuum depends not only on the strain field at the same point but also on strains at all other points of the body. Therefore, the nonlocal stress tensor at the point $x$ is defined by [52]

$$\sigma(x)=\int_V K\left(|x'-x|,\mu\right)T(x')dV(x') \tag{1}$$

$$T(x)=C(x):\varepsilon(x) \tag{2}$$

where $T(x')$ is the classical macroscopic stress tensor at the point, $x$, and $K(|x'-x|,\tau)$ is the nonlocal modulus or debilitation function combining into constitutive equations the nonlocal effects at the reference point $x$ produced by local strain at the source $x'$, $C(x)$ is the fourth-order elasticity tensor, $\varepsilon(x)$ is the strain tensor. $\mu$ Is the material constant which is characterized by $\mu=(e_0a)^2$, where, $e_0$ is a constant related to each material, $a$ is the internal characteristic length. It is hard to solve the elasticity equations using the integral constitutive relation. Therefore, Eringen [36] determines a simplified constitutive relation in a differential form [36]:

$$\left(1-\mu\nabla^2\right)\sigma=T,\quad \mu=(e_0a)^2 \tag{3}$$

where $\nabla$ is the Laplacian operator. For a beam type structure, the nonlocal function can be disregarded along the thickness. So, for a homogeneous and isotropic beam, the fundamental nonlocal equation, according the Euler–Bernoulli theory, can be obtain as the following form [36]:

$$\sigma(x)-(e_0a)^2\frac{\partial^2\sigma(x)}{\partial x^2}=E\,\varepsilon(x) \tag{4}$$

where $E$ is the modulus of elasticity and $e_0a=0$ is nonlocal parameter. Neglecting the rotary of inertia, the equation of motion for the free vibrating Euler–Bernoulli beam has the following form [37, 38]

$$\frac{\partial S}{\partial x}=\rho A\frac{\partial^2 w}{\partial t^2} \tag{5}$$

where $\rho$ is the mass density of the beam, $A$ is the area of the cross-section, $w$ is the transverse deflection of the beam, $t$ denotes the time, $s$ is the shear force and the moment equilibrium condition produces the following equation [53, 54].

$$S=\frac{\partial M}{\partial x} \tag{6}$$

where $M$ is the resultant bending moment which is defined by

$$M=\int_A z\,\sigma(x)dA \tag{7}$$

The axial strain $\varepsilon$ for the Euler–Bernoulli beam is given by

$$\varepsilon(x)=-z\frac{\partial^2 w}{\partial x^2} \tag{8}$$

The bending moment for the nonlocal model, from relations (4), (7) and (8), takes the following form

$$M=-(e_0a)^2\frac{\partial^2 M}{\partial x^2}=-EI\frac{\partial^2 w}{\partial x^2} \tag{9}$$

where $I=\int_A z^2dA$ is the moment of inertia. The clear expression of the nonlocal bending moment can be obtained by substituting Eq. (5) into Eq. (9) and considering Eq. (6) as:

$$M=-EI\frac{\partial^2 w}{\partial x^2}+(e_0a)^2\rho A\frac{\partial^2 w}{\partial t^2} \tag{10}$$

Using Eqs.(5), (6) and (10), the equation of the motion for the nonlocal Euler–Bernoulli beam model in terms of the transverse displacement takes the following form:

$$EI\frac{\partial^4 w(x,t)}{\partial x^4}+\rho A\frac{\partial^2 w(x,t)}{\partial t^2}-\mu\rho A\frac{\partial^4 w(x,t)}{\partial x^2\partial t^2}=0 \tag{11}$$

Likewise, nonlocal torsional vibrations for a beam presented by the following equation:

$$GI_P\frac{\partial^2\theta(x,t)}{\partial x^2}-\rho I_P\frac{\partial^2\theta(x,t)}{\partial t^2}+\mu\rho I_P\frac{\partial^4 w(x,t)}{\partial x^2\partial t^2}=0 \tag{12}$$

where $\theta$ and $I_p$ are angular displacement and polar moment of inertia and $G$ is the shear modulus and $\gamma$ is the shear strain.

## 4 COUPLED FLEXURAL AND TORSIONAL VIBRATIONS

It is convenient for the subsequent analysis to cast the equations of motion in dimensionless form. Fig. 1 describes the geometry definitions of the U-shaped AFM probe. All spatial dimensions including the coordinates $x$, $y$ , and $z$ , and the displacements are defined in relation with the length $L$ of the legs of the system as well as the probe geometry and are denoted by a tilde:

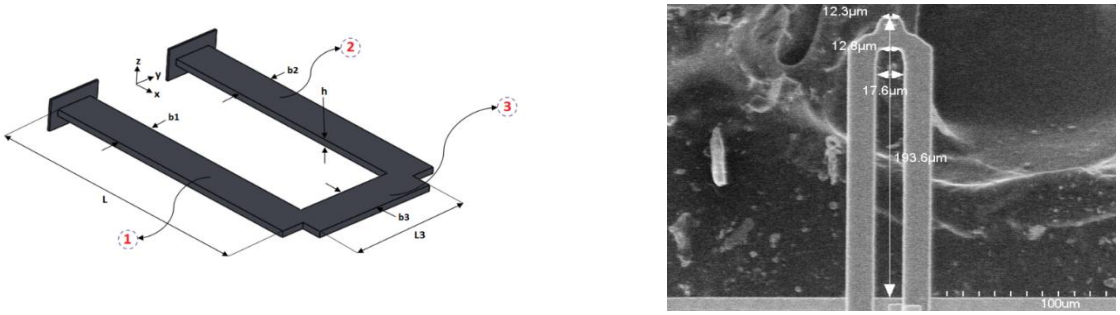


**Fig.1**
Geometry definitions of a U-shaped AFM probe.

$$\tilde{w}_1 = \frac{w}{L_1} \quad ; \quad \tilde{w}_2 = \frac{w}{L_2} \quad ; \tilde{w}_1 = \frac{w}{L_1}; \quad \tilde{x} = \frac{x}{L} \; ; \quad \tilde{L}_3 = \frac{L_3}{L_1}; \quad \tilde{y} = \frac{y}{L_3}. \tag{13}$$

In addition, a dimensionless time $\tau$ is defined as:

$$\tau = t\sqrt{\frac{(EI)_1}{(\rho A)_1 L^4}}. \tag{14}$$

Finally, the dimensionless equations of flexural and torsional motions for the three beams of the system are given by

$$\frac{\partial^4 \tilde{w}_1}{\partial \tilde{x}^4} + \frac{\partial^2 \tilde{w}_1}{\partial \tau^2} - \frac{\mu_1}{L^2_1}\frac{\partial^4 \tilde{w}_1}{\partial \tilde{x}^2 \partial \tau^2} = 0 \tag{15}$$

$$\frac{\partial^4 \tilde{w}_2}{\partial \tilde{x}^4} + \frac{(E\,I)_1(\rho A)_2 L^4_2}{(E\,I)_2(\rho A)_1 L^4_1}\frac{\partial^2 \tilde{w}_1}{\partial \tau^2} - \mu_2 \frac{(E\,I)_1(\rho A)_2 L^2_2}{(E\,I)_2(\rho A)_1 L^4_1}\frac{\partial^4 \tilde{w}_2}{\partial \tilde{x}^2 \partial \tau^2} = 0 \tag{16}$$

$$\frac{\partial^4 \tilde{w}_3}{\partial \tilde{y}^4} + \frac{(E\,I)_1(\rho A)_3 L^4_3}{(E\,I)_3(\rho A)_1 L^4_1}\frac{\partial^2 \tilde{w}_3}{\partial \tau^2} - \mu_3 \frac{(E\,I)_1(\rho A)_3 L^2_3}{(E\,I)_3(\rho A)_1 L^4_1}\frac{\partial^4 \tilde{w}_3}{\partial \tilde{y}^2 \partial \tau^2} = 0 \tag{17}$$

$$\frac{\partial^2 \tilde{\theta}_1}{\partial \tilde{x}^2} + \frac{(\mu\rho)_1(E\,I)_1}{(\rho A)_1 G_1 L^4_1}\frac{\partial^4 \tilde{\theta}_1}{\partial \tilde{x}^2 \partial \tau^2} - \frac{\rho(E\,I)_1 L^2_1}{(\rho A)_1 G_1 L^4_1}\frac{\partial^2 \tilde{\theta}_1}{\partial \tau^2} = 0 \tag{18}$$

$$\frac{\partial^2\tilde{\theta}_2}{\partial\tilde{x}^2}+\frac{(\mu\rho)_2(E\,I)_1}{(\rho A)_1G_1L_1^4}\frac{\partial^4\tilde{\theta}_2}{\partial\tilde{x}^2\partial\tau^2}-\frac{\rho(E\,I)_1L_2^2}{(\rho A)_1G_1L_1^4}\frac{\partial^2\tilde{\theta}_2}{\partial\tau^2}=0 \tag{19}$$

$$\frac{\partial^2\tilde{\theta}_3}{\partial\tilde{y}^2}+\frac{(\mu\rho)_3(E\,I)_1}{(\rho A)_1G_1L_1^4}\frac{\partial^4\tilde{\theta}_3}{\partial\tilde{y}^2\partial\tau^2}-\frac{\rho(E\,I)_1L^2_3}{(\rho A)_1G_1L_1^4}\frac{\partial^2\tilde{\theta}_3}{\partial\tau^2}=0 \tag{20}$$

The parallel beams are clamped at one end and are connected to the cross beam at another end. The boundary conditions at the clamped ends are given by

$$\tilde{w}_1(0,\tau)=0 \tag{21}$$

$$\frac{\partial\tilde{w}_1(0,\tau)}{\partial\tilde{x}}=0 \tag{22}$$

$$\tilde{\theta}_1(0,\tau)=0 \tag{23}$$

$$\tilde{w}_2(0,\tau)=0 \tag{24}$$

$$\frac{\partial\tilde{w}_2(0,\tau)}{\partial\tilde{x}}=0 \tag{25}$$

$$\tilde{\theta}_2(0,\tau)=0 \tag{26}$$

$$\tilde{w}_1(1,\tau)=\tilde{L}_3\tilde{w}_3(-\frac{1}{2},\tau). \tag{27}$$

$$\tilde{w}_1'(1,\tau)=\tilde{\theta}_3(-\frac{1}{2},\tau) \tag{28}$$

$$\tilde{\theta}_1(1,\tau)=\tilde{w}_3'(-\frac{1}{2},\tau). \tag{29}$$

$$\tilde{w}_2(1,\tau)=\tilde{L}_3\tilde{w}_3(\frac{1}{2},\tau) \tag{30}$$

$$\tilde{w}_2'(1,\tau)=\tilde{\theta}_3(\frac{1}{2},\tau) \tag{31}$$

$$\tilde{\theta}_2(1,\tau)=\tilde{w}_3'(\frac{1}{2},\tau) \tag{32}$$

The balance on forces and momentums for the first leg and the cross beam;

$$\frac{(E\,I)_1}{L^2_1}\tilde{w}_1'''(1,\tau)-\frac{(E\,I)_3}{L^2_3}\tilde{w}_3'''(-\frac{1}{2},\tau)=0 \tag{33}$$

$$\frac{(GJ)_1}{L_1}\tilde{\theta}_1'(1,\tau)-\frac{(EI)_3}{L_3}\tilde{w}_3'''(-\frac{1}{2},\tau)=0 \tag{34}$$

$$\frac{(EI)_1}{L_1}\tilde{w}_1''(1,\tau)-\frac{(GJ)_3}{L_3}\tilde{\theta}_3'(-\frac{1}{2},\tau)=0 \tag{35}$$

Likewise, the force and moment balance for the second leg and the cross beam is given by

$$\frac{(EI)_2}{L_2^2}\tilde{w}_2'''(1,\tau)+\frac{(EI)_3}{L_3^2}\tilde{w}_3'''(\frac{1}{2},\tau)=0 \tag{36}$$

$$\frac{(GJ)_2}{L_2}\tilde{\theta}_2'(1,\tau)+\frac{(EI)_3}{L_3}\tilde{w}_3'''(\frac{1}{2},\tau)=0 \tag{37}$$

$$\frac{(EI)_2}{L_2}\tilde{w}_2''(1,\tau)+\frac{(GJ)_3}{L_3}\tilde{\theta}_3'(\frac{1}{2},\tau)=0 \tag{38}$$

Eqs. (21) through (38) define all the boundary and continuity conditions for the probe. It should be noted that this model matches the conditions for the three beams only at a single point. However, it will be shown that this approach captures the salient aspects of the dynamics of the system in terms of the resonant frequencies and the mode shapes.

*4.1 Solutions*

Separating the variables, the governing equations given by Eqs. (15-20) can be solved. For example, for the flexural motion of leg 1, we seek solutions of the form

$$\tilde{w_1}(\tilde{x},\tau)=X_1(\tilde{x}).\cos(\tilde{\omega}\tau) \tag{39}$$

where $X_1$ and $\cos(\tilde{\omega}\tau)$ are functions only of a single independent variable, $\tilde{x}$ or $\tau$, respectively. Substituting this form into the governing equation, the governing ordinary differential equation is found as:

$$X''''(\tilde{x})+\tilde{\omega}^2\frac{\mu}{L_1^2}X''(\tilde{x})-\tilde{\omega}^2X(\tilde{x})=0 \tag{40}$$

That defines the relation between the dimensionless frequency and dimensionless wavenumber. The general solution of this equation is given by

$$X_1(\tilde{x})=C_{11}\sinh(M_1\tilde{x})+C_{21}\cosh(M_1\tilde{x})+C_{31}\sin(M_2\tilde{x})+C_{41}\cos(M_2\tilde{x}) \tag{41}$$

A similar set of solutions is obtained for each of the six equations given by Eqs. (15-20). It should be noted that the entire beam oscillates at the same frequency for a given mode, so, the time dependence is identical for each equation. However, the wave numbers for the flexural and torsional motions are different for each beam. The boundary conditions at the clamped end of the legs allow the spatial dependence of the flexure to be written as:

$$X_1(\tilde{x})=C_{11}\sinh(M_1\tilde{x})+C_{21}\cosh(M_1\tilde{x})+C_{31}\sin(M_2\tilde{x})+C_{41}\cos(M_2\tilde{x}) \tag{42}$$

$$X_2(\tilde{x})=C_{12}\sinh(M_1\tilde{x})+C_{22}\cosh(M_1\tilde{x})+C_{32}\sin(M_2\tilde{x})+C_{42}\cos(M_2\tilde{x}) \tag{43}$$

$$X_3(\tilde{y}) = C_{13}\sinh(M_3\tilde{y}) + C_{23}\cosh(M_3\tilde{y}) + C_{33}\sin(M_4\tilde{y}) + C_{43}\cos(M_4\tilde{y}) \tag{44}$$

and the spatial dependence for the torsional motion:

$$\theta_1(\tilde{x}) = E_{11}\sin(M_5\tilde{x}) + E_{21}\cos(M_5\tilde{x}) \tag{45}$$

$$\theta_2(\tilde{x}) = E_{12}\sin(M_5\tilde{x}) + E_{21}\cos(M_5\tilde{x}) \tag{46}$$

$$\theta_3(\tilde{y}) = E_{13}\sin(M_6\tilde{y}) + E_{23}\cos(M_6\tilde{y}) \tag{47}$$

The wave numbers are given in Eqs. (42-47) are all related to $\omega$ by the relations

$$M_1 = \pm\sqrt{\frac{1}{2}(-\tilde{\omega}^2\frac{\mu_1}{L_1^2})^2 + \sqrt{(\tilde{\omega}^2\frac{\mu_1}{L_1^2})^2 + 4\tilde{\omega}^2}} \tag{48}$$

$$M_2 = \pm i\sqrt{\frac{1}{2}(\tilde{\omega}^2\frac{\mu_1}{L_1^2})^2 + \sqrt{(\tilde{\omega}^2\frac{\mu_1}{L_1^2})^2 + 4\tilde{\omega}^2}} \tag{49}$$

$$M_3 = \pm\sqrt{\frac{1}{2}(-\tilde{\omega}^2\mu_3\frac{L_3^2}{L_1^4} \pm \sqrt{(\tilde{\omega}^2\mu_3\frac{L_3^2}{L_1^4})^2 + 4\tilde{\omega}^2\frac{L_3^4}{L_1^4}})} \tag{50}$$

$$M_4 = \pm i\sqrt{\frac{1}{2}(\tilde{\omega}^2\mu_3\frac{L_3^2}{L_1^4} \pm \sqrt{(\tilde{\omega}^2\mu_3\frac{L_3^2}{L_1^4})^2 + 4\tilde{\omega}^2\frac{L_3^4}{L_1^4}})} \tag{51}$$

$$M_5 = \sqrt{\frac{(\tilde{\omega}^2\frac{\rho(EI)_1}{(\rho A)_1 G_1 L_1^2})}{(1-\frac{(\mu\rho)_1(EI)_1}{(\rho A)_1 G_1 L_1^4}\tilde{\omega}^2)}} \tag{52}$$

$$M_6 = \sqrt{\frac{(\tilde{\omega}^2\frac{\rho(EI)_1}{(\rho A)_1 G_3 L_1^2}L^2{}_3)}{(1-\frac{(\mu\rho)_3(EI)_1}{(\rho A)_1 G_3 L_1^4}\tilde{\omega}^2)}} \tag{53}$$

Finally, it is should be noted that the relation between the wavenumber and the frequency (in *Hz*) is given by

$$f = \frac{1}{2\pi}\sqrt{\frac{(EI)_1}{(\rho A)_1}}\frac{\tilde{\omega}^2}{L^2}. \tag{54}$$

The set of spatial functions given in Eqs. (42-47) includes twelve unknown coefficients. Eqs. (21-38) give the eighteen conditions provide a set of eighteen equations for eighteen unknowns that define the solution space for the TBM. They comprise a homogeneous 18×18 system of equations that can be written as a matrix of the trigonometric functions and geometric parameters multiplying a vector of the unknown coefficients. The determinant of the matrix gives a characteristic equation and the solution of which gives the infinite set of allowable wave numbers for the probe and thus the frequencies from Eq. (54). Each wave number also defines a unique probe mode shapes. In such a system, the flexural and torsional motions of the three beams are coupled. As with all types of such eigenvalue problems [35], each mode shape can be found only within a multiplicative constant.

## 5 RESULTS AND DISCUSSION

Table 1. shows the dimensionless frequency, $\tilde{\omega}$ to free vibrational U-shape probes. To verify the accuracy of the results, dimensionless frequencies of U-shape probes are compared with results presented by Rezaei [40]. Dimensionless natural frequencies $\tilde{\omega}$ of U-shape probes are represented in Table 1. for various values of thickness ratios and nonlocal parameter, $\mu$. It should be noted that, $\mu = 0$ corresponds to local beam theory. As it can be seen, the results of the present theory are in high agreement with those found by Rezaei [40] for all values of thickness ratios, where, the nonlocal parameter is equal to zero.

**Table 1**
Comparison of results for dimensionless frequency $\tilde{\omega}$, for local case ( $\mu = 0$ ) of U- shaped probe.

| Mode shape | Cantilever | Present | Rezaei[40] |
|---|---|---|---|
| 1st Flexural symmetry | A | 2.9617 | 2.9584 |
| | B | 2.9247 | 2.9241 |
| | C | 3.2697 | 3.2761 |
| 2nd Flexural symmetry | A | 19.3136 | 19.2721 |
| | B | 19.0977 | 19.0969 |
| | C | 20.6576 | 20.6146 |
| 3rd Flexural symmetry | A | 55.1608 | 54.9081 |
| | B | 54.1172 | 54.4644 |
| | C | 58.1842 | 58.0644 |
| 4th Flexural symmetry | A | 109.2050 | 112.3600 |
| | B | 108.1350 | 106.0900 |
| | C | 114.5690 | 114.4900 |

In order to know the effect of relative parameters on the natural frequency of probes, the material properties of a silicon wafer with crystallographic of direction is considered as follows: $E = 150GPa, G = 65GPa, \rho = 2329Kg/m^3, \nu = 0.25.$ In order to validate the results, five different types of U-shaped probes are selected (see Fig. 2), and each geometry is given in Table 2. Note that, the real probes are not perfectly U-shaped, as it is assumed. However, the goal of this work is to test the local frequencies of TBM with respect to nonlocal results for realistic and representative probe geometry.

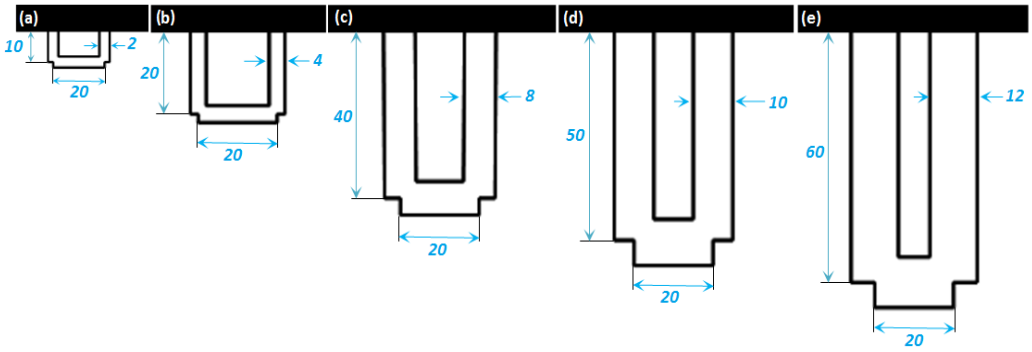


**Fig.2**
Three different types of examined U-shaped probes (dimensions in nanometers).

Table 1. shows the dimensionless geometry values for the selected probes (for probes *a, b, c, d* and *e*, the length scale $(L_1/L_3)$ is 0.5, 1, 2, 2.5 and 3, respectively). Because the thickness of probes can be difficult to assess without the use of electron microscopy, one goal is to evaluate the sensitivity of the results to the thickness.

**Table 2**
Dimensionless geometries of the studied cantilevers (See Fig. 3 for an explanation of the geometry).

| Cantilever | $\tilde{L}_3$ | $\tilde{h}$ | $\tilde{b}$ |
|---|---|---|---|
| | 2 | 0.1 | 0.2 |
| *a* | 2 | 0.05 | 0.1 |
| | 2 | 0.02 | 0.04 |
| | 1 | 0.1 | 0.2 |
| *b* | 1 | 0.05 | 0.1 |
| | 1 | 0.02 | 0.04 |
| | 0.5 | 0.1 | 0.2 |
| *c* | 0.5 | 0.05 | 0.1 |
| | 0.5 | 0.02 | 0.04 |
| | 0.4 | 0.1 | 0.2 |
| *d* | 0.4 | 0.05 | 0.1 |
| | 0.4 | 0.02 | 0.04 |
| | 0.33 | 0.1 | 0.2 |
| *e* | 0.33 | 0.05 | 0.1 |
| | 0.33 | 0.02 | 0.04 |

As it is seen in Table 2., the probes are selected in such a way that they cover a wide range of possible geometries relative to the length of the "legs" (*L*). The probe *b* has equal legs with its cross beam. The longitudinal of these probes (Fig. 2) have $L_1/h=10$. These geometrical differences are expected to influence the vibrational characteristics. The TBM assumes the probe consists of five beams and each beam can be deformed individually in different ways and in both flexure and twisting motion. Therefore, several mode shapes can be imagined. For this type of probe, the mode shapes are identified based on the relative motion of the legs for the TBM. First, note that the legs can be oscillated synchronously or asynchronously.

Tables 3 to 5 exhibit the effect of the nonlocal parameter on incitement frequency to first three modes of the U-shape probes. The response of higher modes can be ignored to purpose more verify the present results, the first three vibration frequencies of a U-shape probe with various aspect ratios $L_1/h=10,\ 20,\ 50$ and $L_3=20nm$ have been investigated and the results are compared with the results of local. It should be noted that $\mu=0$ corresponds to the local beam theory. Here, the small-scale effect can be expressed by the nonlocal parameter $\mu=(e_0a)^2$, and the frequencies are non-dimensionalized by Eq. (54). In these tables, it is shown, rising of the nonlocal parameter decreases the frequencies of U-shape probes. When the value of $L_1/h$ increases, the nonlocal parameter effect on the frequencies decreases. It is shown that, for a U-shape probe with a certain aspect ratio, frequencies decrease with increasing in nonlocal effect and increase with mode number increases. For example, probe (a), when $L_1/h=10$ and $\mu=1,2,3,4$ the decrements are 0.12%, 0.23%, 0.34%, 0.47, respectively, for the first mode, and the decrements are 0.54%, 1.20%, 1.98%, 2.82%, respectively, for the second mode, and the decrements are 2.71%, 4.89%, 7.87%, 10.90%, respectively, for the third mode. The reason of this action is, small wavelength make the small-scale effect more considerable for higher vibration modes of the probe. Following explanation is presented as:

$$\left[(\tilde{\omega}^{local}-\tilde{\omega}^{nonlocal})/\tilde{\omega}^{local}\right]\times 100\%)$$

**Table 3**
The dimensionless frequencies for the first mode of the U-shape probes.

| Nonlocal parameter($\mu$) | $L_1 / h$ | Cantilever | | | | |
|---|---|---|---|---|---|---|
| | | *a* | *b* | *c* | *d* | *e* |
| 0 | 10 | 1.4677 | 1.9973 | 2.4698 | 2.60707 | 2.71180 |
| | 20 | 1.4706 | 2.007 | 2.4739 | 2.61085 | 2.7135 |
| | 50 | 1.4718 | 2.0029 | 2.4750 | 2.61190 | 2.71629 |
| 1 | 10 | 1.4660 | 1.9970 | 2.4698 | 2.60705 | 2.71179 |
| | 20 | 1.4693 | 2.0014 | 2.4738 | 2.61083 | 2.71530 |
| | 50 | 1.4702 | 2.0026 | 2.4750 | 2.61188 | 2.71628 |
| 2 | 10 | 1.4643 | 1.9967 | 2.4697 | 2.60703 | 2.71179 |
| | 20 | 1.4676 | 2.0011 | 2.4738 | 2.61081 | 2.71529 |
| | 50 | 1.4685 | 2.0023 | 2.4749 | 2.61187 | 2.71627 |
| 3 | 10 | 1.4626 | 1.9963 | 2.4697 | 2.60701 | 2.71177 |
| | 20 | 1.4658 | 2.0007 | 2.4737 | 2.61078 | 2.71527 |
| | 50 | 1.4667 | 2.0019 | 2.4749 | 2.61184 | 2.61625 |
| 4 | 10 | 1.4607 | 1.9959 | 1.4696 | 2.60698 | 2.71175 |
| | 20 | 1.4639 | 2.0003 | 2.4737 | 2.61075 | 2.71624 |
| | 50 | 1.4648 | 2.0015 | 2.4748 | 2.61181 | 2.71624 |

**Table 4**
The dimensionless frequencies for the second mode of the U-shape probes.

| Nonlocal parameter($\mu$) | $L_1 / h$ | Cantilever | | | | |
|---|---|---|---|---|---|---|
| | | *a* | *b* | *c* | *d* | *e* |
| 0 | 10 | 3.25525 | 5.26802 | 8.98448 | 10.6562 | 12.1490 |
| | 20 | 3.25753 | 5.27933 | 9.08643 | 10.8386 | 12.4206 |
| | 50 | 3.25817 | 5.28249 | 9.11495 | 10.8896 | 12.4960 |
| 1 | 10 | 3.23770 | 5.25860 | 8.9801 | 10.6530 | 12.1467 |
| | 20 | 3.23991 | 5.26978 | 9.08181 | 10.8353 | 12.4172 |
| | 50 | 3.24053 | 5.27290 | 9.11025 | 10.8862 | 12.4931 |
| 2 | 10 | 3.21596 | 5.24612 | 8.97371 | 10.6482 | 12.1430 |
| | 20 | 3.21810 | 5.25712 | 9.07497 | 10.8299 | 12.4130 |
| | 50 | 3.2169 | 5.26019 | 9.10329 | 10.8807 | 12.4891 |
| 3 | 10 | 3.19061 | 5.23071 | 8.96520 | 10.4619 | 12.1379 |
| | 20 | 3.19264 | 5.24151 | 9.06590 | 10.8225 | 12.4081 |
| | 50 | 3.19321 | 5.24452 | 9.099407 | 10.8732 | 12.4831 |
| 4 | 10 | 3.16220 | 5.21256 | 8.95475 | 10.6333 | 12.1313 |
| | 20 | 3.16413 | 5.22312 | 9.08569 | 10.8135 | 12.4006 |
| | 50 | 3.16467 | 5.22606 | 9.08269 | 10.8638 | 12.4753 |

**Table 5**
The dimensionless frequencies for the third mode of the U-shape probes.

| Nonlocal parameter($\mu$) | $L_1 / h$ | Cantilever | | | | |
|---|---|---|---|---|---|---|
| | | *a* | *b* | *c* | *d* | *e* |
| 0 | 10 | 6.22442 | 14.2499 | 17.1560 | 17.6727 | 18.0625 |
| | 20 | 6.25729 | 14.5426 | 17.5344 | 18.0081 | 18.3628 |
| | 50 | 6.26616 | 14.6216 | 17.6396 | 18.1015 | 18.4466 |
| 1 | 10 | 6.08908 | 14.1040 | 17.1385 | 17.6664 | 18.0582 |
| | 20 | 6.11936 | 14.3800 | 17.51448 | 17.9991 | 18.3552 |
| | 50 | 6.12753 | 14.4544 | 17.6195 | 18.0923 | 18.4418 |
| 2 | 10 | 5.91966 | 13.8182 | 17.0953 | 17.6441 | 18.0473 |
| | 20 | 5.94607 | 14.0659 | 17.4663 | 17.9767 | 18.3463 |
| | 50 | 5.95319 | 14.1325 | 17.5692 | 18.0692 | 18.4296 |
| 3 | 10 | 5.73402 | 13.4495 | 17.0278 | 17.6120 | 18.0301 |
| | 20 | 5.75634 | 13.6661 | 17.3904 | 17.9410 | 18.3275 |
| | 50 | 5.76236 | 13.7243 | 17.7243 | 18.0325 | 18.4103 |
| 4 | 10 | 5.54540 | 13.0473 | 13.0473 | 17.5685 | 18.0066 |
| | 20 | 5.56403 | 13.2355 | 13.2355 | 17.8929 | 18.3018 |
| | 50 | 5.56906 | 13.2859 | 13.2859 | 17.3872 | 18.3840 |

Fig.3 shows the first to third dimensionless frequencies with respect to selected aspect ratios ($L_1/L_3=0.5,1,2,25,3$) for $L_1/h=10$. It is seen that in all curves, by increasing the aspect ratio, the dimensionless frequency increases, but the effect of aspect ratios on the third mode shape is greater than the first and the second mode shape. According to this figure, it is discerned that increase in the cross-beam ($L_3$) length decreases the dimensionless frequency.

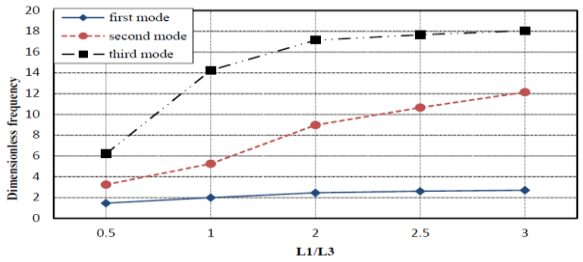


**Fig.3**
The effect of the cross beam length on dimensionless frequencies for $L_1/h=10$.

Figs. 4-8 clearly show the fundamental dimensionless frequencies for various thicknesses of the U-shaped beam considering five various values of the nonlocal parameter($\mu=0,1,2,3,4$) and for different values of the aspect ratios ($L_1/L_3=0.5$ , 1 , 2 , 2.5 , 3). As it is evident from the figures, the results of dimensionless frequencies considering the nonlocal model effect are lower than those of local (classical).Another observation from the figures is that the dimensionless frequencies of the beam are such that, as aspect ratio becomes lower, the nonlocal effect will be severe.

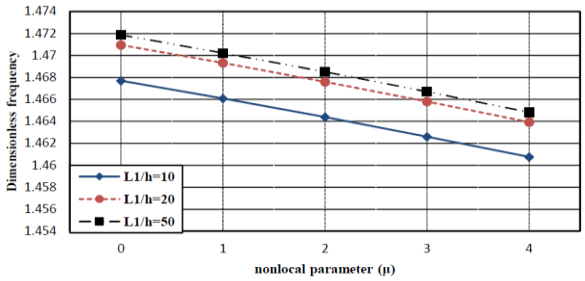


**Fig.4**
The effect of the nonlocal parameter and the beam thickness on fundamental dimensionless frequencies for $L_1/L_3=0.5$.

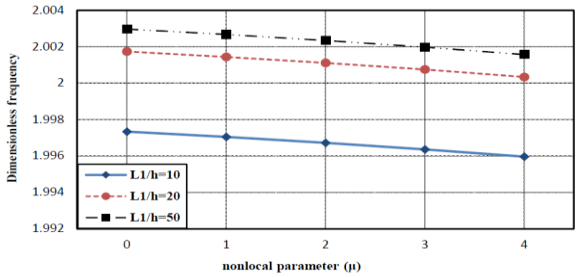


**Fig.5**
The effect of the nonlocal parameter and the beam thickness on fundamental dimensionless frequencies for $L_1/L_3=1$.

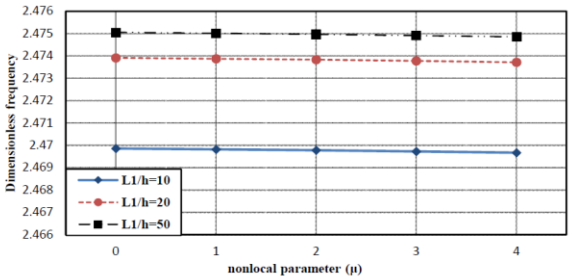


**Fig.6**
The effect of the nonlocal parameter and the beam thickness on fundamental dimensionless frequencies for $L_1/L_3=2$.

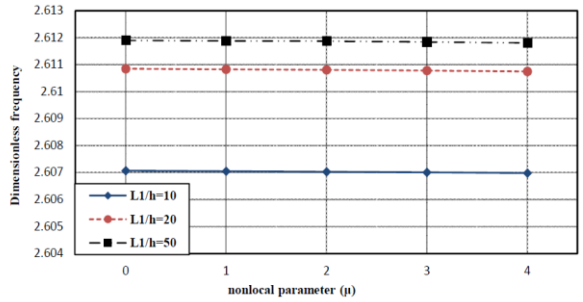


**Fig.7**
The effect of the nonlocal parameter and the beam thickness on fundamental dimensionless frequencies for $L_1 / L_3 = 2.5$.

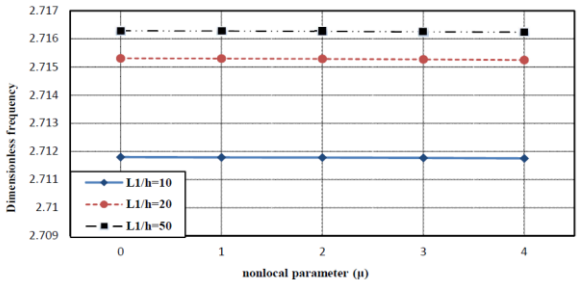


**Fig.8**
The effect of the nonlocal parameter and the beam thickness on fundamental dimensionless frequencies for $L_1 / L_3 = 3$.

The most important observation from Figs. 4-8 is that, for the beam with a certain aspect ratio, the fundamental dimensionless frequencies go up as the thickness decreases.

## 6 CONCLUSIONS

In this article, the transverse vibration of the U-shaped probe was analyzed utilizing Euler-Bernoulli beam model. Governing equations and boundary conditions were derived by separation method. Results are presented to show the length scale parameter, the beam length $(L_1)$, and the thickness $(h)$ effects on the beam. Observations represented that, increasing the aspect ratio $(L/h)$ of the probe increases the dimensionless frequencies. In addition, the beam length $(L_1)$ will be more effective on higher frequencies.

In this article, it has been shown that the TBM appears to be reliable for a wide range of geometries, and it can be applied to almost all the probes, which have a similar shape. The value of the frequency is directly related to the aspect ratio, $(L/h)$ of the probe and obviously is higher for thicker probes. In contrast with single-beam probes, the mode shapes of the U-shaped probes are a complex combination of bending and twisting motions, especially for higher modes. Such a complex behavior Creates tension for using such probes for dynamic imaging techniques like contact resonance AFM. The initial model needs to be adjusted and iterated to match the experimental results with possible remeshing at each iteration step. Limitations of probe manufacturing imply that this process needs to be repeated for each probe. In this case, contact resonance techniques would not be possible. The analytical form of the TBM provides the needed accuracy and computational efficiency to make such calculations possible. The model represented here can be extended to include tip-sample coupling as well this work is now underway. This aspect of the problem will also introduce an additional coupling mechanism for different types of vibration behaviors compounding the complexity of the inverse analysis. The efficiency of the TBM for inversion of experimental contact resonance frequency data as a means of quantifying sample elastic and/or viscoelastic properties remains to be determined, but this approach is likely to be valuable for such materials characterization measurements.

## REFERENCES

[1] Rogers B., 2003, High speed tapping mode atomic force microscopy in liquid using an insulated piezoelectric cantilever, *Review of Scientific Instruments* **74**(11): 4683-4686.

[2] Giessibl F.J., 1998, High-speed force sensor for force microscopy and profilometry utilizing a quartz tuning fork, *Applied Physics Letters* **73**(26): 3956-3958.

[3] Tortonese M., Barrett R., Quate C., 1993, Atomic resolution with an atomic force microscope using piezoresistive detection, *Applied Physics Letters* **62**(8): 834-836.
[4] Lin S., 2005, Measurements of the forces in protein interactions with atomic force microscopy, *Current Proteomics* **2**(1): 55-81.
[5] Fung R. F., Huang S. C., 2001, Dynamic modeling and vibration analysis of the atomic force microscope, *Journal of Vibration and Acoustics* **123**(4): 502-509.
[6] Colton R.J., 2004, Nanoscale measurements and manipulation, *Journal of Vacuum Science & Technology B* **22**(4): 1609-1635.
[7] Jalili N., Laxminarayana K., 2004, A review of atomic force microscopy imaging systems: application to molecular metrology and biological sciences, *Mechatronics* **14**(8): 907-945.
[8] Rabe U., Turner J., Arnold W., 1998, Analysis of the high-frequency response of atomic force microscope cantilevers, *Applied Physics A: Materials Science & Processing* **66**: S277-S282.
[9] Yamanaka K., 2001, Resonance frequency and Q factor mapping by ultrasonic atomic force microscopy, *Applied Physics Letters* **78**(13): 1939-1941.
[10] Johnson K.L., 1987, *Contact Mechanics*, Cambridge University Press.
[11] Rabe U., Janser K., Arnold W., 1996, Vibrations of free and surface-coupled atomic force microscope cantilevers: Theory and experiment, *Review of Scientific Instruments* **67**(9): 3281-3293.
[12] Turner J.A., 1997, High-frequency response of atomic-force microscope cantilevers, *Journal of Applied Physics* **82**(3): 966-979.
[13] Turner J.A., Wiehn J.S., 2001, Sensitivity of flexural and torsional vibration modes of atomic force microscope cantilevers to surface stiffness variations, *Nanotechnology* **12**(3): 322.
[14] Chang W. J., 2002, Sensitivity of vibration modes of atomic force microscope cantilevers in continuous surface contact, *Nanotechnology* **13**(4): 510.
[15] Yamanaka K., Nakano S., 1998, Quantitative elasticity evaluation by contact resonance in an atomic force microscope, *Applied Physics A: Materials Science & Processing* **66**: S313-S317.
[16] Hurley D., Turner J.A., 2004, Humidity effects on the determination of elastic properties by atomic force acoustic microscopy, *Journal of Applied Physics* **95**(5): 2403-2407.
[17] Rabe U., 2000, Quantitative determination of contact stiffness using atomic force acoustic microscopy, *Ultrasonics* **38**(1): 430-437.
[18] Rodriguez B.J., 2007, Dual-frequency resonance-tracking atomic force microscopy, *Nanotechnology* **18**(47): 475504.
[19] Rabe U., 2002, Imaging and measurement of local mechanical material properties by atomic force acoustic microscopy, *Surface and Interface Analysis* **33**(2): 65-70.
[20] Gannepalli A., 2011, Mapping nanoscale elasticity and dissipation using dual frequency contact resonance AFM, *Nanotechnology* **22**(35): 355705.
[21] Jesse S., 2007, The band excitation method in scanning probe microscopy for rapid mapping of energy dissipation on the nanoscale, *Nanotechnology* **18**(43): 435503.
[22] Amelio S., 2001, Measurements of elastic properties of ultra-thin diamond-like carbon coatings using atomic force acoustic microscopy, *Thin Solid Films* **392**(1): 75-84.
[23] Stan G., 2009, Contact-resonance atomic force microscopy for nanoscale elastic property measurements: spectroscopy and imaging, *Ultramicroscopy* **109**(8): 929-936.
[24] Stan G., Cook R., 2008, Mapping the elastic properties of granular Au films by contact resonance atomic force microscopy, *Nanotechnology* **19**(23): 235701.
[25] Mahdavi M.H., Farshidianfar A., Dalir H.,2006, High frequency analysis of a non-contact atomic force microscopy microcantilever, *in 14th Annual (International) Mechanical Engineering Conference,* Isfahan University of Technology.
[26] Barretta R., de Sciarra F.M., 2015, Analogies between nonlocal and local Bernoulli–Euler nanobeams, *Archive of Applied Mechanics* **85**(1): 89-99.
[27] Romano G., 2017, Constitutive boundary conditions and paradoxes in nonlocal elastic nanobeams, *International Journal of Mechanical Sciences* **121**: 151-156.
[28] Romano G., Barretta R., 2016, Exact solution of Eringen's nonlocal integral model for bending of Euler–Bernoulli and Timoshenko beams , *International Journal of Engineering Science* **109**: 240-242.
[29] Demir C., Civalek Ö., 2013, Torsional and longitudinal frequency and wave response of microtubules based on the nonlocal continuum and nonlocal discrete models, *Applied Mathematical Modelling* **37**(22): 9355-9367.
[30] Gao X., 2015, A new Timoshenko beam model incorporating microstructure and surface energy effects, *Acta Mechanica* **226**(2): 457.
[31] Civalek Ö., Akgöz B., 2009, Static analysis of single walled carbon nanotubes (SWCNT) based on Eringen's nonlocal elasticity theory, *International Journal of Engineering and Applied Sciences* **1**(2): 47-56.
[32] Abbasi M., Mohammadi A.K., 2010, A new model for investigating the flexural vibration of an atomic force microscope cantilever, *Ultramicroscopy* **110**(11): 1374-1379.
[33] Akgöz B., Civalek Ö., 2014, A new trigonometric beam model for buckling of strain gradient microbeams, *International Journal of Mechanical Sciences* **81**: 88-94.

[34] Civalek Ö., Akgöz B., 2013, Vibration analysis of micro-scaled sector shaped graphene surrounded by an elastic matrix, *Computational Materials Science* **77**: 295-303.
[35] Lee H. L., Chang W. J., 2008, Coupled lateral bending–torsional vibration sensitivity of atomic force microscope cantilever, *Ultramicroscopy* **108**(8): 707-711.
[36] Muraoka M., 2005, Sensitivity-enhanced atomic force acoustic microscopy with concentrated-mass cantilevers, *Nanotechnology* **16**(4): 542.
[37] Challamel N., Wang C., 2008, The small length scale effect for a non-local cantilever beam: a paradox solved, *Nanotechnology* **19**(34): 345703.
[38] Lim C., Li C., Yu J., 2009, The effects of stiffness strengthening nonlocal stress and axial tension on free vibration of cantilever nanobeams, *Interaction and Multiscale Mechanics: an International Journal* **2**(3): 223-233.
[39] Narendar S., 2012, Differential quadrature based nonlocal flapwise bending vibration analysis of rotating nanotube with consideration of transverse shear deformation and rotary inertia, *Applied Mathematics and Computation* **219**(3): 1232-1243.
[40] Rezaei E., Turner J., 2014, Free vibrations of U-shaped atomic force microscope probes, *Journal of Applied Physics* **115**(17): 174302.
[41] Meirovitch L., Parker R., 2001, Fundamentals of vibrations, *Applied Mechanics Reviews* **54**: 100.
[42] Aydogdu M., 2009, Axial vibration of the nanorods with the nonlocal continuum rod model, *Physica E: Low-Dimensional Systems and Nanostructures* **41**(5): 861-864.
[43] Idzuchi H., Fukuma Y., Otani Y., 2015, Spin transport in non-magnetic nano-structures induced by non-local spin injection, *Physica E: Low-Dimensional Systems and Nanostructures* **68**: 239-263.
[44] Sarrami-Foroushani S., Azhari M., 2014, Nonlocal vibration and buckling analysis of single and multi-layered graphene sheets using finite strip method including van der Waals effects, *Physica E: Low-Dimensional Systems and Nanostructures* **57**: 83-95.
[45] Salehipour H., Nahvi H., Shahidi A., 2015, Exact analytical solution for free vibration of functionally graded micro/nanoplates via three-dimensional nonlocal elasticity, *Physica E: Low-Dimensional Systems and Nanostructures* **66**: 350-358.
[46] Ansari R., 2015, Free vibration of fractional viscoelastic Timoshenko nanobeams using the nonlocal elasticity theory, *Physica E: Low-Dimensional Systems and Nanostructures* **74**: 318-327.
[47] Ke L. L., Wang Y. S., 2014, Free vibration of size-dependent magneto-electro-elastic nanobeams based on the nonlocal theory, *Physica E: Low-Dimensional Systems and Nanostructures* **63**: 52-61.
[48] Kiani K., 2014, Nonlocal continuous models for forced vibration analysis of two-and three-dimensional ensembles of single-walled carbon nanotubes, *Physica E: Low-Dimensional Systems and Nanostructures* **60**: 229-245.
[49] Adhikari S., Murmu T., McCarthy M., 2014, Frequency domain analysis of nonlocal rods embedded in an elastic medium, *Physica E: Low-Dimensional Systems and Nanostructures* **59**: 33-40.
[50] Wang L., 2009, Vibration and instability analysis of tubular nano-and micro-beams conveying fluid using nonlocal elastic theory, *Physica E: Low-Dimensional Systems and Nanostructures* **41**(10): 1835-1840.
[51] Yang J., Ke L., Kitipornchai S., 2010, Nonlinear free vibration of single-walled carbon nanotubes using nonlocal Timoshenko beam theory, *Physica E: Low-Dimensional Systems and Nanostructures* **42**(5): 1727-1735.
[52] Eringen A.C., 1983, On differential equations of nonlocal elasticity and solutions of screw dislocation and surface waves, *Journal of Applied Physics* **54**(9): 4703-4710.
[53] Zhang Y., Liu G., Xie X., 2005, Free transverse vibrations of double-walled carbon nanotubes using a theory of nonlocal elasticity, *Physical Review B* **71**(19): 195404.
[54] Lu P., 2006, Dynamic properties of flexural beams using a nonlocal elasticity model, *Journal of Applied Physics* **99**(7): 073510.